HEAT, MOMENTUM AND MOISTURE BUDGETS OF THE KATABATIC LAYER OVER THE MELTING ZONE OF THE WEST GREENLAND ICE SHEET IN SUMMER

MICHIEL R. VAN DEN BROEKE,[1] PETER G. DUYNKERKE[1] and EDWIN A. C. HENNEKEN[2]
[1]*Institute for Marine and Atmospheric Research Utrecht, Utrecht University, Utrecht, The Netherlands;* [2]*Faculty of Earth Sciences, Free University, Amsterdam, The Netherlands*

(Received in final form 6 May, 1994)

Abstract. The budgets of momentum, heat and moisture of the atmospheric boundary layer overlying the melting zone of the west Greenland ice sheet during an 8-day period in summer are calculated. To do so, the governing budget equations are derived and presented in terms of vertically averaged quantities. Moreover, stationarity is assumed in the present study. Measurements collected during the GIMEX-91 experiment are used to calculate the contribution of the different terms in the equations to the budget.

During summer, a well developed katabatic wind system is present over the melting zone of the Greenland ice sheet. The budgets show that advection in the katabatic layer is small for momentum, heat and humidity, when the horizontal length scale of the integration area is sufficiently large (>50 km). This indicates that in principle one-dimensional atmospheric models can be used to study the boundary layer over the melting zone of the Greenland ice sheet. The background stratification plays a crucial role in the heat and moisture budget. Vertical divergence of longwave radiation provides one-third and the turbulent flux of sensible heat the rest of the cooling of the boundary layer. Moisture is added to the boundary layer by evaporation which is a significant term in the moisture budget. Negative buoyancy (katabatic forcing) dominates the momentum budget in the downslope direction. Coriolis forcing is important, stressing the large spatial scale of the katabatic winds on the Greenland ice sheet.

1. Introduction

The integrated mass balance of glaciers and ice caps is of direct influence to mean global sea level (Oerlemans and Fortuin, 1992; Oerlemans, 1993). The structure of the atmospheric boundary layer (ABL) over ice and snow determines the surface energy budget through the turbulent fluxes of heat and moisture. Therefore the ABL is important for the mass balance (net gain/loss of mass) of that particular snow/ice surface. This paper aims to describe the different processes that determine bulk characteristics of the steady state ABL over the melting zone of the Greenland ice sheet, as observed during GIMEX-91 (Greenland Ice Margin EXperiment). During GIMEX, surface-layer characteristics were measured using 6 m high masts while vertical profiles were obtained with a tethered balloon and RASS/SODAR equipment.

Since ice (formed through pressurisation of accumulated snow) is a plastic material, it tends to stream away from the main accumulation area, resulting in sloping surfaces. When air overlying the sloping surface is cooled (either by longwave radiation divergence or sensible heat flux), a horizontal pressure

Boundary-Layer Meteorology **71:** 393–413, 1994.

gradient is established and the air starts to slow down the slope. The resulting wind is called 'katabatic flow', and it occurs in all stable ABLs overlying sloping surfaces.

Glacier winds occur when air with a temperature larger than 0 °C is advected over a melting glacier surface. Turbulent cooling of the air by the melting ice surface results in a down-glacier directed flow component. As stated above, the development of these winds is one of the factors determining the amount of melt and they have been well described (Streten *et al.*, 1974; Munro and Davies 1978; Stenning *et al.*, 1981; Ohata, 1989a; Ohata, 1989b).

Undoubtedly the most violent katabatic winds can be found in the coastal areas of the Antarctic continent. The topography has a continental length scale owing to the lens-shaped ice cap. The drainage of large amounts of radiatively cooled air from the high plateau results in the highest values of mean wind speed and directional constancy found on earth, with the direction and strength of the flow depending strongly on direction and steepness of the slope. Farther inland, so-called inversion winds prevail. These are also down-slope winds, but with a large component across the fall line, caused by increased influence of Coriolis forcing owing to the more gentle slopes in these areas. Altogether, Antarctic katabatic winds have received much attention, theoretically as well as experimentally (Ball, 1956; Loewe, 1974; Ohata *et al.*, 1985; Sorbjan *et al.*, 1986; Parish and Waight, 1987; Heinemann, 1988; Kottmeier, 1988; Kodama *et al.*, 1989; King, 1989; Pettré and André, 1991; Parish and Bromwich, 1991; Gallée and Schayes, 1992). Although no melt occurs on Antarctica (except at some spots on the Antarctic peninsula), katabatic winds still influence the mass balance through enhanced evaporation of snow and divergence of drifting snow transport.

In contrast to the Antarctic ice sheet, the ice sheet melt in Greenland determines about half the yearly loss of mass (Ambach, 1977; Greuell, 1992; Van de Wal and Oerlemans, 1994), the other half being calving of icebergs. The most interesting difference with Antarctica is that, owing to the melting surface, the boundary layer over melting ice remains stably stratified during strong insolation in the day time, whereas in the Antarctic it becomes unstable and the katabatic force vanishes (Wendler *et al.*, 1988). The presence of an approximately 100 km wide, almost two-dimensional melting area, bordered on one side by bare tundra and on the other side by dry snow offers a unique opportunity to study the dynamics and thermodynamics of the boundary layer (Loewe, 1935; Schwerdtfeger, 1972). Close to the ice margin, one quarter to one third of the melting energy is provided by the sensible heat flux. Evaporation of water from the surface is especially important higher up the ice where net radiation is smaller owing to increasing reflectivity of the surface (Henneken *et al.*, 1994; Van de Wal and Russell, 1994; Duynkerke and Van den Broeke, 1994). Furthermore it was found that heating of the ABL over the tundra during daytime creates a tremendous horizontal temperature gradient, locally accelerating the katabatic layer. At night the opposite occurs and the flow is locally decelerated (Van den Broeke *et al.*, 1994).

The first results of recent meteorological research in Greenland are described in a special issue of *Global and Planetary Change*, number 9, 1994.

2. Suitable Equations for Katabatic Flow

2.1. General budget equations with assumptions

We assume two-dimensionality setting all y-derivatives to zero, except for the large-scale pressure gradient. The positive x-direction is defined in the up-slope (west-east) direction; the positive y-axis points in the south-north direction. The different terms should be in suitable form for calculation using the data collected during the experiment. Mostly we shall follow the approach of Mahrt (1982). We partition the dependent variables according to:

$$\phi^* = \phi_0(z) + \phi + \phi', \tag{1}$$

where the zero subscript refers to the background state not influenced by the downslope flow, while ϕ is the mean value of the variable owing to the katabatic flow and the accent denotes turbulent fluctuations from the mean. The undisturbed background state is assumed to be horizontally homogeneous and stationary. The potential temperature and specific humidity distribution depends only on altitude and the deviations from this background state are $f(t, x, z)$, while the geostrophic wind is assumed constant with height throughout the boundary layer. The general Equations (2) to (7) describe the conservation of momentum, heat, moisture and mass of the mean variables in turbulent flow.

$$\frac{\partial u}{\partial t} + u\frac{\partial u}{\partial x} + w\frac{\partial u}{\partial z} = -\frac{1}{\rho_r}\frac{\partial p}{\partial x} + f(v - v_g) - \frac{\partial(\overline{w'u'})}{\partial z}, \tag{2}$$

$$\frac{\partial v}{\partial t} + u\frac{\partial v}{\partial x} + w\frac{\partial v}{\partial z} = -f(u - u_g) - \frac{\partial(\overline{w'v'})}{\partial z}, \tag{3}$$

$$-\frac{1}{\rho_r}\frac{\partial p}{\partial z} = g\frac{\theta}{\theta_r}, \tag{4}$$

$$\frac{\partial \theta}{\partial t} + u\frac{\partial(\theta + \theta_0)}{\partial x} + w\frac{\partial(\theta + \theta_0)}{\partial z} = -\frac{\partial(\overline{w'\theta'})}{\partial z} - \frac{1}{\rho_r c_p}\frac{\partial F}{\partial z}, \tag{5}$$

$$\frac{\partial q}{\partial t} + u\frac{\partial(q + q_0)}{\partial x} + w\frac{\partial(q + q_0)}{\partial z} = -\frac{\partial(\overline{w'q'})}{\partial z}, \tag{6}$$

$$\frac{\partial u}{\partial x} + \frac{\partial w}{\partial z} = 0, \tag{7}$$

where in Equations (2) and (3) u, v and w are the velocity components in the x, y and z direction, respectively; f is the Coriolis parameter ($f = 1.4 * 10^{-4}$

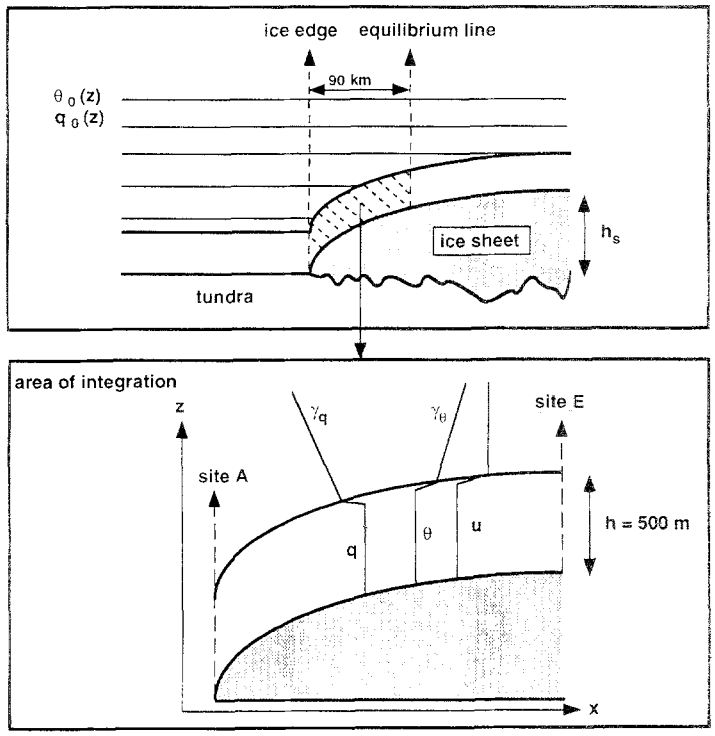

Fig. 1. The area of integration in the present budget study (hatched area in the upper panel) is bounded from below by the melting ice surface and from above by a fixed level above the ice surface $h_s + h$, where h is set to 500 m in the present study. The left and right borders are defined by the position of the ice edge (site A) and the equilibrium line (site E), respectively. In the second panel the area of integration is enlarged, and schematic profiles of u, θ and q are shown.

s^{-1}), and the subscript g denotes geostrophic wind components. In Equation (3) θ is defined as the deviation of potential temperature from the background state according to Equation (1), which in katabatic flow is negative by definition. F represents the net upward longwave radiation. Specific humidity is represented by q. The reference potential temperature θ_r and density ρ_r are chosen to be 290 K and 1.15 kg m^{-3}, respectively. The other symbols have their usual meteorological meanings. The x axis is aligned horizontally, and points in the slope direction (Figure 1), while the z-axis is aligned vertically (note that Mahrt defines the x-axis parallel to the surface and the z-axis normal to the surface). This has the direct advantage that the background potential temperature state $\theta_0(z)$ is a function of height only. The height of the topography is $h_s(x)$ and the thickness of the katabatic layer h. The ice edge is aligned perpendicular to the downslope direction. The ablation zone is bordered by dashed arrows in Figure 1. It extends from the ice edge (site A) to the equilibrium line (site E, where the mass balance equals zero) and is approximately 90 km wide during the summer in this part of Greenland.

The hydrostatic Equation (4) can be integrated in the z-direction to an undisturbed level $h_s + h$ somewhere above the top of the slope flow ($\theta_{h_s+h} = 0$ K and the driving force disappears, i.e., $p_{h_s+h} = 0$) and then differentiated with respect to x to obtain an expression for the downslope pressure gradient:

$$-\frac{1}{\rho_r}\frac{\partial p}{\partial x} = \frac{g}{\theta_r}\frac{\partial(\widehat{\theta}_z h)}{\partial x}. \tag{8}$$

The temperature deviation in this expression is a function of z and is defined by Mahrt as averaged over the depth of the layer between z ($z \geq h_s$) and $h_s + h$:

$$\frac{1}{h - z'}\int_z^{h_s+h} \theta \, \mathrm{d}z' \equiv \widehat{\theta}_z, \tag{9}$$

and equals the layer-averaged temperature deviation for $z \to 0$. Upon substitution of Equation (8) into Equation (2), we find for the momentum equation in the x-direction:

$$\frac{\partial u}{\partial t} + u\frac{\partial u}{\partial x} + w\frac{\partial u}{\partial z} = \frac{g}{\theta_r}\frac{\partial(\widehat{\theta}_z h)}{\partial x} + f(v - v_g) - \frac{\partial(\overline{w'u'})}{\partial z}. \tag{10}$$

2.2. Hydraulic approximation

For convenience and in order to relate the observed structure of the boundary layer to the different terms of the heat, mass and momentum budgets, we shall use the hydraulic approach, also used by, e.g., Manins and Sawford (1979). This means that we shall treat the katabatic layer as a layer without vertical structure. This approach is justified since we are only interested in bulk momentum, heat and moisture budgets of the boundary layer in this study, and not so much in the detailed vertical distribution of the different variables. In order to obtain the equivalent mean variables, we integrate all terms from the ice surface h_s to a constant level above the surface h_s+h. Let the double bar for any depth-integrated independent variable ξ be defined by:

$$\frac{1}{h}\int_{h_s}^{h_s+h} \xi \, \mathrm{d}z \equiv \overline{\overline{\xi}}. \tag{11}$$

Averaging over a layer in the present orientation of the axes requires the use of Leibniz's theorem:

$$\int_{h_s}^{h_s+h}\left[\frac{\partial \xi}{\partial x}\right]\mathrm{d}z = \frac{\partial}{\partial x}\left[\int_{h_s}^{h_s+h} \xi \, \mathrm{d}z\right] - \xi_{h_s+h}\frac{\partial(h_s + h)}{\partial x} + \xi_{h_s}\frac{\partial h_s}{\partial x}. \tag{12}$$

Writing the budget equations for heat and momentum in flux form, adding the continuity Equation (7), and applying Leibniz's theorem, we arrive at the flux form of the equations for vertically-averaged variables in the katabatic layer:

$$\frac{\partial(\overline{\overline{u}}h)}{\partial t} + \frac{\partial(\overline{\overline{u}\overline{u}}h)}{\partial x} = \int_{h_s}^{h_s+h} \left[\frac{g}{\theta_r}\frac{\partial(\hat{\theta}_z h)}{\partial x}\right] \mathrm{d}z + \\ + fh(\overline{\overline{v}} - \overline{\overline{v_g}}) - [(\overline{w'u'})_{h_s+h} - (\overline{w'u'})_{h_s}], \tag{13}$$

$$\frac{\partial(\overline{\overline{v}}h)}{\partial t} + \frac{\partial(\overline{\overline{u}\overline{v}}h)}{\partial x} = -fh(\overline{\overline{u}} - \overline{\overline{u_g}}) - [(\overline{w'v'})_{h_s+h} - (\overline{w'v'})_{h_s}], \tag{14}$$

$$\frac{\partial(\overline{\overline{\theta}}h)}{\partial t} + \frac{\partial(\overline{\overline{u}\overline{\theta}}h)}{\partial x} + \frac{\partial(\overline{\overline{u}\overline{\theta_0}}h)}{\partial x} + (\theta_0 w)_{h_s+h} \\ = \frac{-1}{\rho_r c_p}(F_{h_s+h} - F_{h_s}) - [(\overline{w'\theta'})_{h_s+h} - (\overline{w'\theta'})_{h_s}] \tag{15}$$

$$\frac{\partial(\overline{\overline{q}}h)}{\partial t} + \frac{\partial(\overline{\overline{u}\overline{q}}h)}{\partial x} + \frac{\partial(\overline{\overline{u}\overline{q_0}}h)}{\partial x} + (q_0 w)_{h_s+h} = -[(\overline{w'q'})_{h_s+h} - (\overline{w'q'})_{h_s}], \tag{16}$$

$$\frac{\partial(\overline{\overline{u}}h)}{\partial x} + w_{h_s+h} = 0. \tag{17}$$

We shall take the integration depth h constant and large enough to assure that the fluxes disappear at the level $h_s + h$ in Equations (13)–(16). Furthermore, we align the x-axis with the axis of the experiment. The next step is writing out the integral in Equation (13) and the last two terms on the left-hand side of Equations (15) and (16). We start with Equation (13):

$$\int_{h_s}^{h_s+h} \left[\frac{g}{\theta_r}\frac{\partial(\hat{\theta}_z h)}{\partial x}\right] \mathrm{d}z = \frac{g}{\overline{\overline{\theta_r}}}\left[\frac{\partial \overline{\overline{\hat{\theta}_z}} h^2}{\partial x} + h\hat{\theta}_{h_s}\frac{\partial h_s}{\partial x} - h\hat{\theta}_{h_s+h}\frac{\partial h_s}{\partial x}\right], \tag{18}$$

where $\hat{\theta}_{h_s} = \overline{\overline{\theta}}$ and $\hat{\theta}_{h_s+h} = 0$. When rewriting the last two terms on the left-hand side of Equations (15) and (16), we use a stationary background potential temperature and specific humidity profile which is linear with height and has a lapse rate γ_ξ (ξ is either θ or q):

$$\xi_{0,z} = \xi_{0,0} + \frac{\mathrm{d}\xi_0}{\mathrm{d}z}z = \xi_{0,0} + \gamma_\xi z \Rightarrow \overline{\overline{\xi_0}} = \xi_{0,h_s+h} - \gamma_\xi \frac{h}{2}. \tag{19}$$

This yields, again using (7):

$$\frac{\partial(\overline{\overline{u}}\overline{\overline{\xi_0}}h)}{\partial x} + (\xi_0 w)_{h_s+h} = \gamma_\xi \left[\overline{\overline{u}}h\frac{\partial h_s}{\partial x} + hw_{h_s+h} + \frac{\partial}{\partial x}\int_0^h \overline{\overline{u}}z'\,\mathrm{d}z'\right] \tag{20}$$

where $z' = z - h_s$, i.e., the height above the surface. All three terms are associated with advection of air, either along the surface (first term between brackets) or through subsidence (second term). The third term is a correction that accounts for uneven distribution of momentum vertically, and will generally be small. Note that all terms on the right-hand side no longer depend on ξ or ξ_0, but only on downslope velocity and background stratification. We substitute Equation (18) into Equations (13) and (20) into Equations (15) and (16), and assume stationarity. We then obtain the integrated budgets for momentum, heat and moisture in 2-dimensional form for a slab of air (Figure 1) with constant depth h and horizontal extent $\mathrm{d}x$, ranging from the ice edge ($x = x_1 = 0$) to the equilibrium line ($x = x_2$):

$$\begin{matrix} & \text{ADV} & & \text{TW} & & \text{KAT} & & \text{COR} & \text{FRIC} \end{matrix}$$

$$\int_{x_1}^{x_2} \mathrm{d}x \left\{ -\frac{\partial(\overline{\overline{uu}}h)}{\partial x} + \frac{g}{\theta_r}\left[\frac{\partial \overline{\overline{\hat{\theta}_z}}h^2}{\partial x} + h\overline{\overline{\theta}}\frac{\partial h_s}{\partial x}\right] + fh(\overline{\overline{v}} - \overline{\overline{v_g}}) + (\overline{w'u'})_{h_s} \right\} = 0, \tag{21}$$

$$\begin{matrix} & \text{ADV} & & \text{COR} & \text{FRIC} \end{matrix}$$

$$\int_{x_1}^{x_2} \mathrm{d}x \left\{ -\frac{\partial(\overline{\overline{uv}}h)}{\partial x} - fh(\overline{\overline{u}} - \overline{\overline{u_g}}) + (\overline{w'v'})h_s \right\} = 0, \tag{22}$$

$$\begin{matrix} & \text{ADV} & & & \text{STRAT}\,(1,2,3) \end{matrix}$$

$$\int_{x_1}^{x_2} \mathrm{d}x \left\{ -\frac{\partial(\overline{\overline{u\theta}}h)}{\partial x} - \gamma_\theta \left[\overline{\overline{u}}h\frac{\partial h_s}{\partial x} + hw_{h_s+h} + \frac{\partial}{\partial x}\int_0^h \overline{\overline{u}}z'\,\mathrm{d}z'\right] \right.$$

$$\begin{matrix} & \text{RAD} & \text{SENS} \end{matrix}$$

$$\left. + \frac{-1}{\rho_r c_p}(F_{h_s+h} - F_{h_s}) + (\overline{w'\theta'})_{h_s} \right\} = 0, \tag{23}$$

$$\begin{matrix} & \text{ADV} & & & \text{STRAT}\,(1,2,3) & & \text{EVAP} \end{matrix}$$

$$\int_{x_1}^{x_2} \mathrm{d}x \left\{ -\frac{\partial(\overline{\overline{uq}}h)}{\partial x} - \gamma_q \left[\overline{\overline{u}}h\frac{\partial h_s}{\partial x} + hw_{h_s+h} + \frac{\partial}{\partial x}\int_0^h \overline{\overline{u}}z'\mathrm{d}z'\right] + (\overline{w'q'})_{h_s} \right\} = 0. \tag{24}$$

Equation (21) states that in stationary conditions, the advection of momentum along the topography (ADV) is balanced by increasing layer thickness downslope and/or temperature deviation (the thermal wind term TW), katabatic forcing by negative buoyancy (KAT), the Coriolis force (COR) and surface friction (FRIC).

Equation (22) represents the balance between advection, Coriolis forcing and friction for the y-component of the boundary-layer wind speed. The equation for heat, Equation (23), states that in stationary conditions, the advection of the temperature deviation (ADV) and the effect of background stratification (STRAT) are balanced by vertical divergence of longwave radiation (RAD) and turbulent cooling through the surface sensible heat flux (SENS). The effect of stable ambient conditions on the development of katabatic flow can be understood as follows: when the air descends (either by following the topography or subsidence), it encounters potentially colder surroundings that act to decrease the potential temperature deficit of the layer. Approximately the same balance applies for moisture in Equation (24) where only the radiation term is omitted. Moisture is added to boundary-layer air by evaporation (EVAP) at the surface.

Given a 2-dimensional experimental configuration, we can use Equations (21)–(24) to calculate the time-averaged contributions of the different terms to the budgets of momentum, heat and moisture of the ABL over the melting zone of the Greenland ice sheet. We need, therefore, at least two locations with vertical profiles of wind vector, potential temperature and specific humidity and some resolution of ground observations in the x-direction in order to estimate average values of surface fluxes.

3. Experimental Set Up and Data Analysis

The area of interest is the melting zone of the Greenland ice sheet near Søndre Strømfjord (67° N, 54° W); see Figure 2. In midsummer, the tundra adjacent to the ice is free of snow, and has a width of 150 km from sea to ice edge. This contributes to long periods of clear and dry weather in the field area, in contrast to the coastal stations where dense fog prevails in summer. The area near Søndre Strømfjord is believed to be the warmest spot in Greenland during July, with daily average temperatures at screen height exceeding 10 °C (Ohmura, 1987). The width of the melting zone at the peak of the melting season is approximately 90 km.

The data used in this paper were collected using the experimental set up as illustrated in Figure 2. At the ice edge, a tethered balloon was operated every three hours, measuring vertical profiles of the wind vector, temperature and humidity up to 1000 m (site A). Balloon data were interpolated to vertical 10 m increments using least squares fitting of data at 40 m intervals. Three surface masts at 2, 8 and 39 km on the ice measured temperature and wind speed at 2 and 6 m (also 0.5 m at site B), wind direction at 6 m and incoming and reflected shortwave radiation at 1.5 m, respectively. Humidity and total radiation were additionally measured at site B. Data were sent to the base camp with radio telemetry. This part of the experiment in the ablation zone was operated by Utrecht University. This experimental set-up has been used successfully on glaciers in the Alps and in Antarctica.

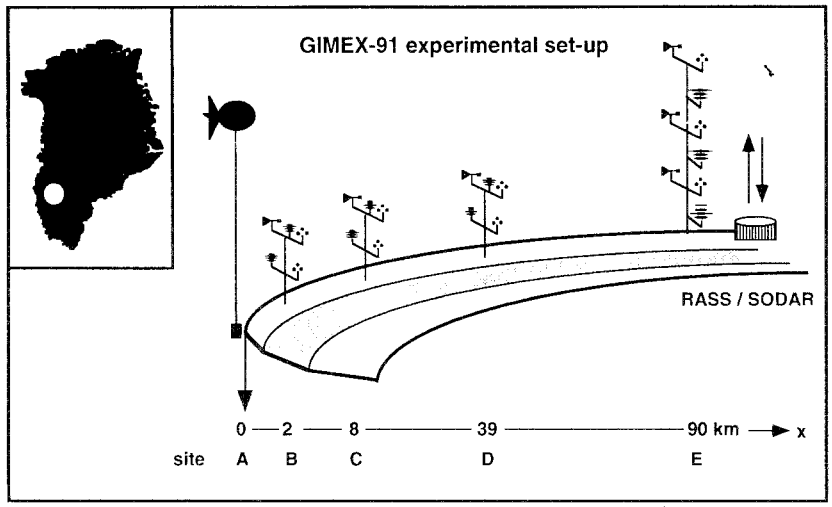

Fig. 2. Schematic overview of the experimental set-up during the Greenland Ice Margin EXperiment (GIMEX) in 1991. The location of the Søndre Strømfjord area is represented by the white dot in the inset.

At the (assumed) equilibrium line site E, 90 km on the ice, a 30 m tower was erected to perform profile measurements of wind speed, temperature and humidity. In addition, the upper part of the boundary layer was sensed from below by RASS (temperature) and SODAR (wind vector). This part of the experiment was operated by the Free University.

Background temperature and humidity profiles were constructed using 12-hourly routine balloon soundings performed at Egedesminde, a coastal station some 200 km farther to the north. In order to remain out of the influence of the katabatic flow, data from 1–4 km altitude were used to determine $\theta_0(z)$ and $q_0(z)$ and extrapolated downward into the ABL to obtain surface values. For a more detailed description of the GIMEX-90/91 expeditions, see Oerlemans and Vugts (1993).

4. Observations

The complete measuring period of GIMEX-91 spanned 52 days (10 June 1991–31 July 1991), but only 35 days of measurements are available of site E (26 June 1991–31 July 1991). In this analysis, the 8-day period from 8 to 15 July 1991 was used. During this period, large-scale forcing appeared to be weak and cloud cover was low.

4.1. General meteorological conditions

July 1991 was characterised by low cloud amounts and weak large-scale circulation in the Søndre Strømfjord area. Nearby stations reported dense fog at the coast throughout this period. Weather somewhat more inland was sunny and warm. To

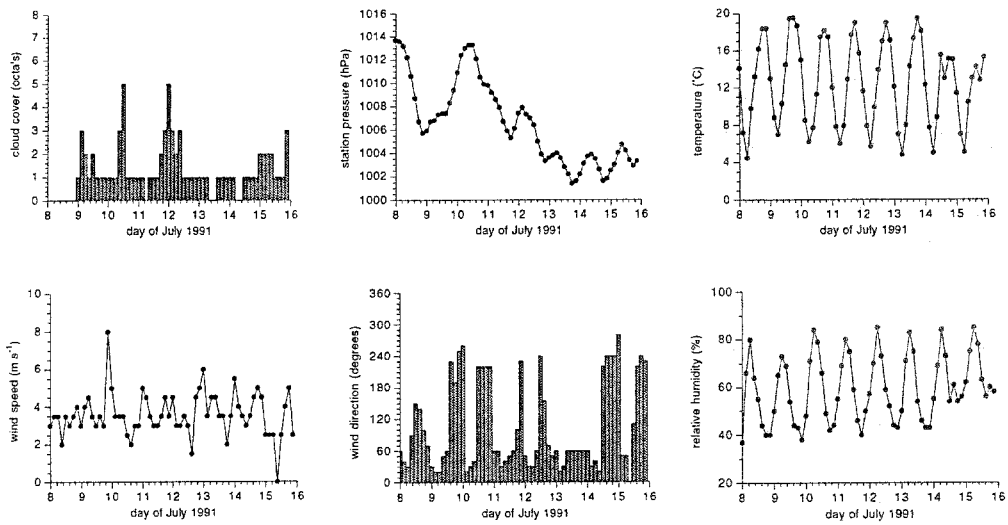

Fig. 3. Three-hourly routine measurements of total cloud amount, pressure, temperature, wind speed and direction and relative humidity at Søndre Strømfjord air base, 20 km to the west of site A.

illustrate this, 3-hrly observations at the airport of Søndre Strømfjord (130 km inland, 20 km away from the ice edge) are presented in Figure 3. Mean cloudiness was close to 1/8; maximum temperatures reached approximately 20 °C in the dry air while the wind was weak, either from the northeast or the southwest. These conditions are believed to be representative for fair summer days in this area, as is confirmed by measurements performed one year earlier during GIMEX-90.

4.2. Average surface-layer observations at sites B, C, D and E

Average 6 m wind speed, 2 m temperature and specific humidity (only site B and E) for the 8-day period under consideration are presented in Figure 4. Figure 4d represents an idealised ice sheet topography and the associated slope angle, using assumptions described in Oerlemans and Van der Veen (1984). The surface height h_s (m.a.s.l.) of the ice sheet is then given by a parabolic profile:

$$h_s = 150 + \left(\frac{2\tau_0 x}{\rho g}\right)^{1/2} = 150 + 4.76\sqrt{x}, \tag{25}$$

where τ_0 represents the ice yield stress (assumed to be constant and 100 kPa), ρ the ice density (900 kg m^{-3}), and x the distance from the ice edge. As can be seen, the snout of the glacier is situated at 150 m.a.s.l. The two-dimensional position of the sites can be described reasonably well by this idealised profile. From Equation (25), the slopes at the different locations of the sites can be calculated, and they range from 12 m km^{-1} at site E to 59 m km^{-1} at site B.

The mean surface wind speed reaches its maximum just before the ice edge (Figure 4a), a location not coinciding with the steepest slope angle. This phe-

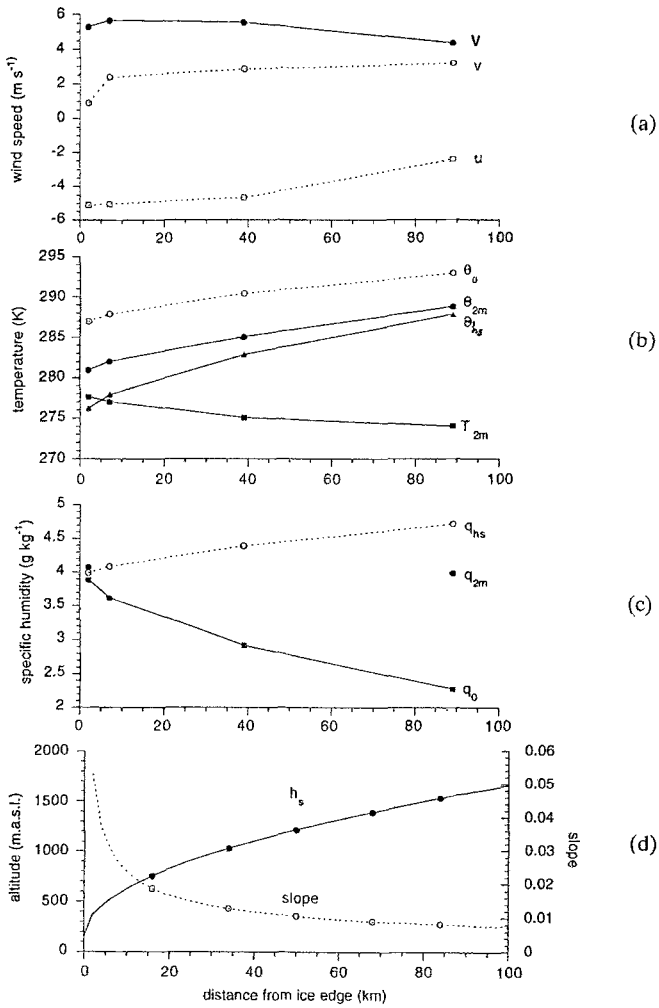

Fig. 4. Average surface quantities above the ice at sites B, C, D and E for the period 8–15 July 1991: (a) 6 m wind speed (V) and down (u), cross (v) slope components; (b) 2 m temperature T_{2m}, 2 m potential temperature θ_{2m}, surface potential temperature θ_{h_s} and background temperature θ_0; (c) 2 m specific humidity q_{2m} (black dots), surface specific humidity (assuming saturation) q_{h_s} and background values at 2 m; (d) idealised ice sheet profile h_s according to Equation (25) (solid line) and corresponding slope (dotted line).

nomenon has also been observed on two-dimensional slopes in Antarctica (Wendler and Kodama, 1985) and is probably due to a thickening of the katabatic layer, indicating that thermal wind effects become increasingly important near the ice edge. The cross-slope component decreases sharply close to the edge, and the surface wind becomes almost fully downslope at site B. This indicates that katabatic forcing or the thermal wind in (21) becomes increasingly important and the Coriolis force negligibly small as slope angle or inversion strength increases.

At site E, the surface flow apparently is balanced by buoyancy, Coriolis and frictional forces, whereas at site B, buoyancy is solely balanced by friction. The directional constancy of the surface wind is defined as the ratio between average scalar wind speed and average vector wind speed. A directional constancy of 1 means that the surface wind blows from one direction all the time. Average values in the ablation zone as observed during GIMEX-91 are typically 0.9 and higher (Van den Broeke *et al.*, 1994), rivalling those of katabatic winds at Antarctica.

Figure 4b shows that the potential temperature at 2 m decreases when descending towards site B, indicating that the boundary layer is stably stratified and the air is cooled near the surface when it flows towards the ice edge. The potential temperature difference between 2 m and the surface increases sharply near the edge. This situation differs strongly from that on Antarctica, where normally the surface potential temperature of the descending air increases or remains constant when the surface inversion weakens through mixing in the summer (Wendler and Kodama, 1985). During the winter, when the ablation zone of the Greenland ice sheet is covered by snow, the thermodynamic situation at the surface on both ice caps will be comparable. Another interesting feature of Figure 4b is the almost constant surface temperature deficit (difference between θ_{2m} and the background state θ_0) as calculated from soundings at Egedesminde (presented in the next section). This indicates on average cooling (turbulent/radiative) and heating (compression and/or entrainment) probably balance near the surface, when following the motion. The slight increase in surface-layer stability when going towards the ice edge in spite of the larger wind speed can be attributed to the fixed surface temperature of 0 °C while the air is adiabatically heated when it is advected down the slope.

Figure 4c shows the background specific humidity values $q_0(z)$ at the different sites together with the surface value q_{h_s} (assuming the air to be saturated and 0 °C at the surface) and observed q_{2m} at sites B and E (black dots). Although the observations are sparse, they suggest that evaporation occurs along the surface profile, and that the evaporation decreases from site E downward towards site B.

With the aid of flux profile relations suggested by Duynkerke (1991), we can calculate the surface sensible and latent heat fluxes at the different sites. Although these relations have proved to be reliable in unstable conditions, their accuracy has not yet been established in the stable boundary layer. However, in the present case, conditions are mostly only moderately stable owing to relatively high wind speeds ($z/L < 1$), during which the flux profile relations have proved to yield reasonable results. The calculated mean values of surface fluxes for momentum, sensible heat and latent heat are presented in Table I. It must be noted that during the period under consideration, site E was still situated over a wet snow surface, and the surface energy balance components at this site are probably not representative for a much larger area in the ablation zone. We shall use an average value for the entire ablation zone of 0.12 m^2 s^{-2} for the downslope momentum flux, a net sensible heat flux at the surface of -46 W m^{-2} (directed

TABLE I

Magnitude of surface fluxes at the different sites for the period 8–15 July 1991.

	Site B	Site C	Site D	Site E
u^* (m s^{-1})	0.23	0.32	0.47	0.26
$\overline{(u'w')}_{h_s}$ (m^2 s^{-2})	0.05	0.09	0.19	0.04
$\overline{(v'w')}_{h_s}$ (m^2 s^{-2})	−0.01	−0.04	−0.11	−0.05
$\overline{(\theta'w')}_{h_s}$ (Km s^{-1})	−0.03	−0.02	−0.06	−0.03
$\overline{(q'w')}_{h_s}$ (m s^{-1})	$6.6 * 10^{-7}$	–	–	$1.2^* 10^{-5}$

towards the surface) and an average latent heat flux of 16 W m^{-2} for the entire ablation zone. These values have been calculated using weighted averages along the masts. The very high values of the friction velocity at site D represents an area with large melting holes and irregularities at the surface, resulting in high flux values, confirming measurements performed in 1990.

4.3. Average vertical profiles

Temperature and humidity profiles obained from 12-hrly balloon soundings performed at Egedesminde were interpolated towards standard altitudes at 25 m intervals and averaged over the period of interest (Figure 5). The assumption of a linear constant background lapse rate for potential temperature seems justified, having a mean value $\partial\theta_0/\partial z$ = +5.1 K km^{-1} in the interval 1–4 km. This value will be used in the rest of this paper. The profiles of specific humidity yielded much more scatter. The moisture content increases sharply towards ground level, and the gradient became strongly negative in the boundary layer at Egedesminde. Analogous to the potential temperature, a background stratification was calculated using the elevation interval 1–4 km, which yielded a value of $\partial q_0/\partial z$ = −0.65 g kg^{-1} km^{-1}. Although the assumption of stationarity and linearity in this case is not as good as for temperature, we shall use this value in the rest of this paper. An analysis of surface weather maps produced an estimate of the geostrophic wind speed components in the Søndre Strømfjord area for this period. They proved to be weak and variable (directional constancy 0.37), but on average from the south: u_g = 0 m s^{-1}, v_g = 3 m s^{-1}. Putnins (1970) states that southerly geostrophic winds prevail over this part of the Greenland ice cap in summer. The above values of the geostrophic flow are included in the COR term of Equation (21).

We can now try to fit the measured boundary-layer profiles at site A and E to the above mentioned background profiles. The available data at both sites are summarised in Table II. All available data have been used to calculate the average profiles. Figure 6a shows the (vector) average vertical profiles of downslope

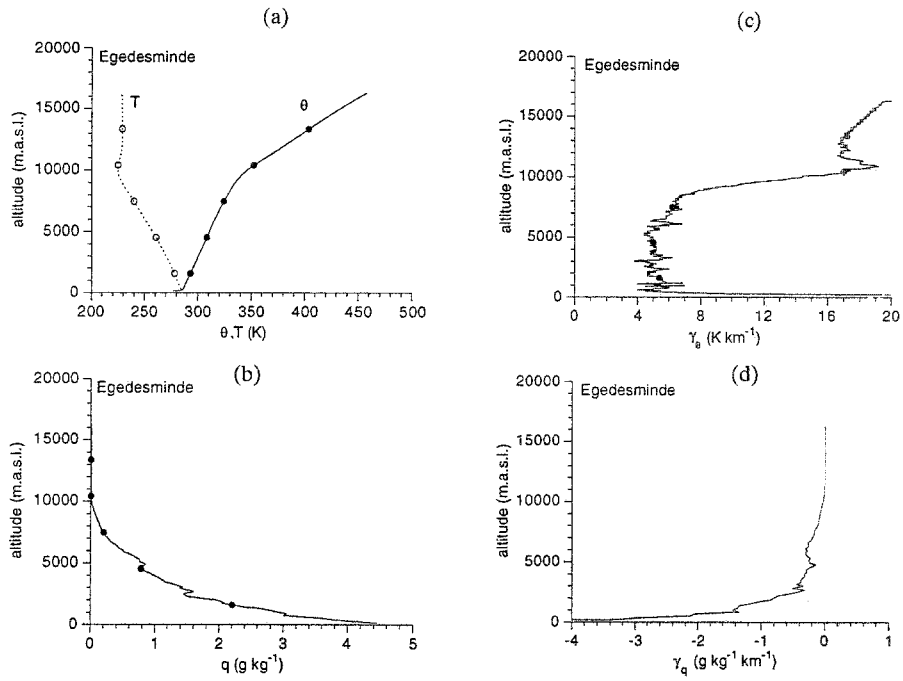

Fig. 5. Average background profiles obtained from balloon soundings at Egedesminde of (potential) temperature (a), potential temperature lapse rate γ_θ (b), specific humidity (c) and smoothed specific humidity lapse rate γ_q (d) for the period 8–15 July 1991.

wind speed u at sites A and E as a function of height above the surface, Figure 6b the directional constancy at site A. Figure 6c shows the averaged potential temperature profile combined with the background profile as a function of altitude above sea level. A cold, surface-based layer can clearly be distinguished, representing the katabatic wind layer. The katabatic wind shows a distinct near-surface maximum at both sites, but the layer is deeper and the wind maximum stronger at the edge (site A), indicating that the katabatic flow develops when descending. This means that significant mass divergence takes place between sites E and A. The peculiar shape of the downslope wind speed profile is caused by vector averaging in time, causing the level with the most persistent wind direction to produce a maximum (Figure 6a). This indicates that the observed wind field is mainly determined by surface cooling.

The altitude above ground level at which the katabatic wind becomes zero coincides well with the altitude at which the temperature deficit becomes zero. Apparently the boundary-layer downslope flow is indeed a thermally driven flow with minor influences from the large-scale pressure gradient, at least during the period considered. Near the ice edge, a weak back flow was observed above the entrainment layer, suggesting the existence of a cell circulation at the ice

TABLE II

Availability of vertical profiles at site A (tethered balloon) and site E (RASS and SODAR) for the period 8–15 July 1991.

Data	Site A (soundings)	Site E (percentage)
8 July	7	100%
9 July	7	17%
10 July	7	33%
11 July	6	96%
12 July	7	96%
13 July	7	0%
14 July	7	96%
15 July	6	33%

edge. This can be expected, because the katabatic forcing disappears above the tundra, and the mass influx into the boundary layer must be compensated at higher altitudes by an easterly flow over a deeper layer.

The importance of longwave radiative cooling for katabatic flows was mentioned earlier by Cerni and Parish (1984) concerning Antarctic katabatic winds. An infrared radiative transfer model of Tjemkes and Duynkerke (1989) has been used to calculate the magnitude of the longwave radiative cooling term at sites A and E in Equation (23). The boundary-layer temperature profiles of Figure 6c have been used together with the mean background profiles as illustrated in Figure 5. Sub-Arctic ozone profiles were obtained from McClatchey (1972). The results of these calculations are presented in Figure 7 (net long-wave radiation, upward positive) as a function of altitude above the surface. The quantity that we are interested in, the net longwave radiative flux divergence over a 500 m thick layer, is 33 W m^{-2} at site A and 8 W m^{-2} at site E. An average value of 21 W m^{-2} for the divergence of long-wave radiation over the horizontal domain was used. When compared to the mean surface cooling of 46 W m^{-2}, this contribution can certainly not be neglected.

The boundary-layer profiles of specific humidity could not be fitted very well with the background profile. This is probably due to external influences at the GIMEX profile or at Egedesminde. However, with certain assumptions, an estimate of the moisture budget can still be made; see next section.

4.4. Application of the budget equations to the observations

In order to estimate the heat and momentum hudget of the boundary layer over the ablation area, the values presented in Table III were derived from the observations

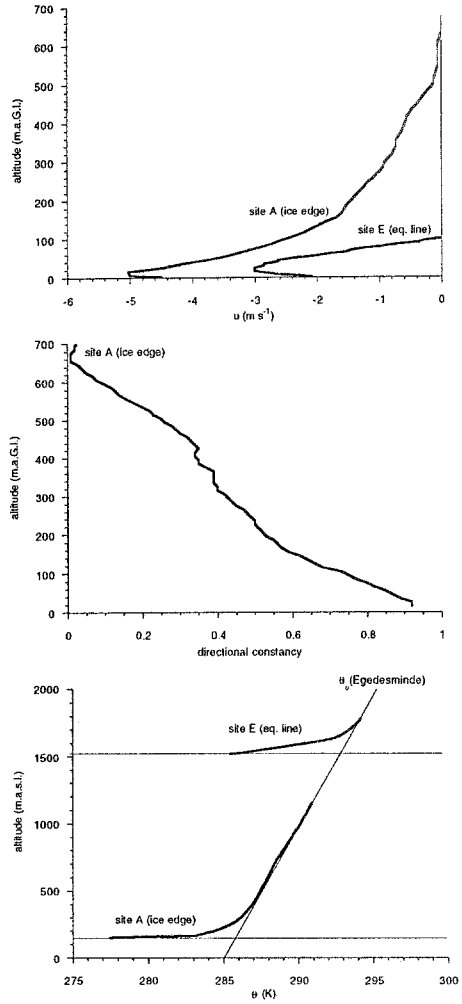

Fig. 6. Average boundary-layer profiles of downslope wind speed (a), directional constancy (b) and potential temperature (c) at sites A and E for the period 8–15 July 1991.

TABLE III

Averaged quantities in the katabatic layer at sites A (ice edge) and E (equilbrium line) for the period 8–15 July 1991.

	$\overline{\overline{u}}$	$\overline{\overline{uu}}$	$\overline{\overline{v}}$	$\overline{\overline{uv}}$	$\overline{\overline{\theta}}$	$\overline{\overline{u\theta}}$	$\overline{\overline{\hat{\theta}}}$
Site A	−1.6	+4.0	+0.7	−1.1	−0.5	+1.7	−0.1
Site E	−0.4	+0.9	+6.5	−2.3	−1.1	+2.1	−0.2

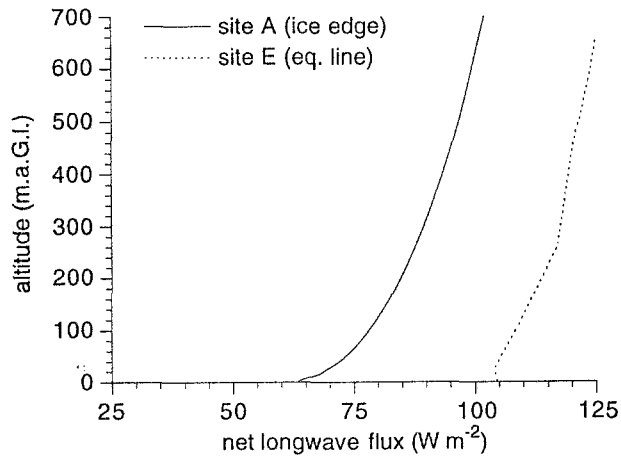

Fig. 7. Calculated profile of net longwave radiation (positive upward) at sites A and E for the period 8–15 July 1991.

described above, using a constant integration depth h = 500 m. The vertical velocity at the level $h_s + h$ was calculated using Equation (17), which yielded w_{h_s+h} = 0.65 cm s^{-1}. This value compares well with those found for instance in Antarctica. Kottmeier (1988) presents values ranging from 0.05 to 2.3 cm s^{-1}. The vertically integrated values of the different quantities are listed in Table III for both sites A and E. It can be seen that the vertically integrated mass flux at site A is about four times larger than at site E, while the temperature deficit is larger at site E.

With the aid of Equations (21)–(25) and Table III, the different terms in the budget equations can now be calculated, the result of which is plotted in Figure 8a–d. The three contributions of the stratification term (STRAT) are numbers 1, 2 and 3 counting from left to right. The imbalance (IMB) in all four budgets is acceptable considering the assumptions made in the previous sections. Since the humidity deviation q could not be calculated, advection was neglected in Equation (24). Since this term is small in the other balances as well, this assumption seems justified, because the resulting imbalance is small in this budget.

As could be expected, the downslope (x) momentum balance of the ABL is dominated by katabatic forcing (Figure 8a), mainly balanced by surface friction and Coriolis forcing, although the latter force is decreased through inclusion of a geostrophic wind of 3 m s^{-1} from the south. The imbalance can be explained by a variation of only 0.5 m s^{-1} in the geostrophic flow, and is therefore acceptable. When integrated over a large (90 km) horizontal area and averaged in time, as we did in this study, the advection and thermal wind terms are unimportant. However, this will not be the case for small time (<1 day) and horizontal length scales (<10 km). It has been shown that the thermal contrast between the boundary layer over the tundra and the ice sheet introduces a thermal wind that dominates the

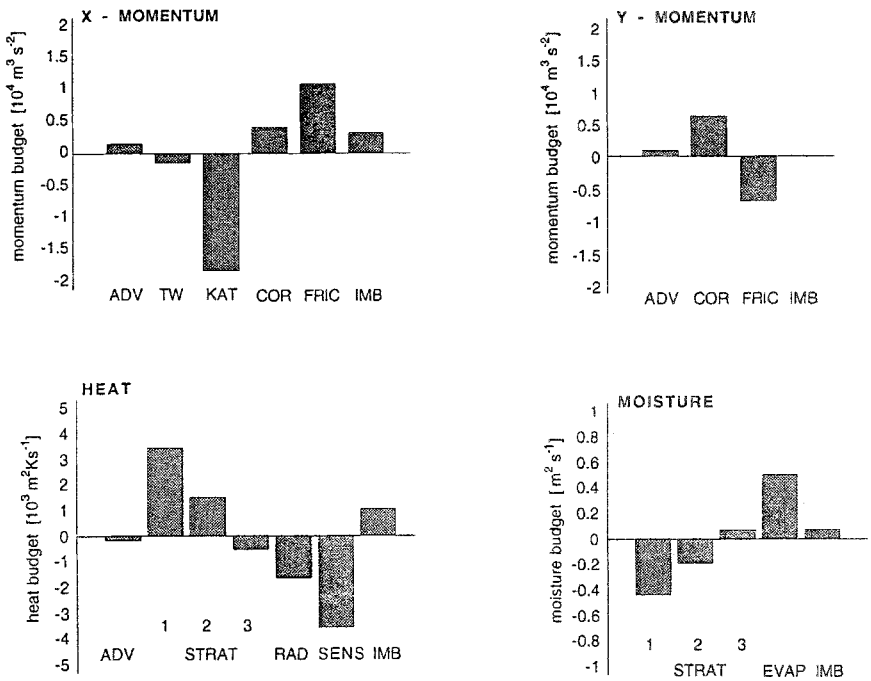

Fig. 8. Budget of momentum (upper) heat (lower left) and moisture (lower right) for the integration area as defined in Figure 1 for the period 8–15 July 1991. See text for further explanation.

local balance close to the edge (Van den Broeke *et al.*, 1994). The y-momentum budget is a simple balance between Coriolis forcing and friction in the present assumption of two-dimensionality.

The background stratification terms (STRAT) of potential temperature and specific humidity acts to increase the amount of heat and decrease the amount of moisture in the katabatic layer over the ice, whenever the downslope velocity is nonzero. According to Figure 8c and d, these processes are mainly compensated by evaporation and downward turbulent transport of heat at the surface. However, longwave radiative cooling is also an important sink of heat of the katabatic layer. The three components of the STRAT term in Equation (23) and (24) are dominated by the term associated with vertical displacement along the topography. The imbalance term in the heat budget could be caused by an overestimated surface heat flux by 13 W m^{-2}. Although in the moisture budget the role of advection could not be calculated, evaporation (EVAP) at the surface probably is the most important source in the moisture budget.

5. Concluding Remarks

The hydraulic approach seems to be an appropriate framework to study the dominant processes of the observed katabatic flow over the melting zone of the Greenland ice sheet. The observed katabatic wind during GIMEX-91 is an extremely persistent phenomenon which completely determines the structure of the ABL overlying the melting zone of the Greenland ice sheet in summer and probably also in winter. The high constancy of the winds indicates continuous stable stratification of boundary-layer air, which is directly linked to the fixed temperature (0 °C) of the melting ice surface and the advection of adiabatically heated air. Other significant features are the turning of the surface wind towards more downslope directions near the ice edge and the importance of the Coriolis force farther on the ice, where the slopes are gentle. The observed katabatic wind field, although some characteristics are quite similar, also shows some interesting differences with its summertime Antarctic counterpart.

Regarding assumptions and uncertainties, the calculated magnitudes of the different terms included in Equations (21)–(24) are reasonably well able to describe the budgets of momentum, heat and moisture of the ABL. The mean vertical profiles of the katabatic layer show the changes as the air is transported down the slope. The layer thickens owing to turbulent entrainment at the top and accelerates in response to the steeper slopes near the ice edge. This leads to significant mass flux divergence in the boundary layer, causing subsidence and heating of boundary-layer air, which is an important production term in the heat balance. When assuming stationarity, entrainment of warm air at the top of the boundary layer compensates subsidence. The estimated magnitude of the entrainment velocity is 0.65 cm s^{-1}, averaged in time and over the ablation zone. Cooling by longwave radiation divergence can not be neglected. The stable background stratification indicates that the undisturbed atmosphere is potentially colder at lower altitudes, which acts to decrease the temperature deficit that drives the katabatic wind. This is confirmed by the smaller temperature deficit at site A compared to site E (Table III). It is furthermore demonstrated that significant evaporation occurs at the surface. Advection is probably small for all the budgets (although for moisture this contribution could not be calculated), which implies that models of the characteristics of the boundary layer overlying the ablation zone of the Greenland ice sheet can be one-dimensional. However, this is only valid for places far away from the ice edge.

Acknowledgements

We thank all members of the GIMEX-90/91 expeditions and meteorologists of the Søndre Strømfjord Weather service for participation and support. Valuable comments were given by J. Oerlemans and A. Meesters. Financial support for this work was obtained from the Dutch National Research Programme on Glob-

al Air Pollution and Climate Change (contract 276/91-NOP), from the Commission of the European Communities (contract EPOC-CT90-0015) and from the Netherlands Organisation for Scientific Research (Werkgemeenschap CO_2-Problematiek).

References

Ambach, W.: 1977, 'Untersuchungen zum energieumsatz in der ablationszone des Grönländische inlandeises', *Expedition Glaciologique Internationale au Groenland* **4**, No. 5, Bianco Lunos Bogtrykkeri A/S, København, pp. 63.

Ball, F. K.: 1956, 'The Theory of Strong Katabatic Winds', *Aust. J. Phys.* **9**, 373–386.

Cerni, T. A. and Parish, T. R.: 1984, 'A Radiative Model of the Stable Nocturnal Boundary Layer with Application to the Polar Night', *J. Clim. Appl. Meteorol.* **22**, 79–91.

Duynkerke, P. G.: 1991, 'Radiation Fog: a Comparison of Model Simulation with Detailed Observations', *Mon. Wea. Rev.* **119**, 324–341.

Duynkerke, P. G. and van den Broeke, M. R.: 1994, 'Surface Energy Balance and Katabatic Flow over Glacier and Tundra during GIMEX-91', *Global and Planetary Change* **9**, 17–28.

Gallée, H. and Schayes, G.: 1992, 'Dynamical Aspects of Katabatic Winds Evolution in the Antarctic Coastal Zone', *Boundary-Layer Meteorol.* **59**, 141–161.

Greuell, W.: 1992, *Numerical Modelling of the Energy Balance and the Englacial Temperature at the ETH Camp*, West Greenland, Zürcher Geographische Schriften 51, ETH Zürich, 81 pp.

Heinemann, G.: 1988, 'On the Structure and Energy Budget of the Boundary Layer in the Vicinity of the Filchner Ronne Ice Shelf Front (Antartica)', *Beitr. Phys. Atmosph.* **61**(3), 244–258.

Henneken, E. A. C., Bink, N. J., Vugts, H. F., Cannemeijer, F., and Meesters, A. G. C. A.: 1994, 'A Case Study of the Daily Energy Balance at the VU-GIMEX Camp', *Global and Planetary Change* **9**, 69–78.

King, J. C.: 1989, 'Low-level Wind Profiles at an Antarctic Coastal Station', *Antarctic Science* **1**(2), 169–178.

Kodama, Y., Wendler, G., and Ishikawa, N.: 1989, 'The Diurnal Variation of the Boundary Layer in Summer in Adélie Land, Eastern Antarctica', *J. Appl. Meteorol.* **28**, 16–24.

Kottmeier, C.: 1988, 'Atmosphärische Strömungsvorgänge am Rande der Antarktis', *Berichte des Institutes für Meteorologie und Klimatologie der Universität Hannover*, Band 33.

Loewe, F.: 1935, 'Das klima des Grönländischen inlandeises', in: *Handbuch der Klimatologie*, **2**(K), 67–101.

Loewe, F.: 1974, 'Considerations Concerning the Winds of Adelie Land', *Zeitschrift für Gletscherkunde und Glazialgeologie* **X**, 189–197.

Mahrt, L.: 1982, 'Momentum Balance of Gravity Flow', *J. Atmos. Sci.* **39**, 2701–2711.

Manins, P. C. and Sawford, B. L.: 1979, 'Katabatic Winds: a Field Case Study', *Q.J.R. Met. Soc.* **105**, 1011–1025.

McClatchey, R. S. W., Fenn, R. W., Selby, J. E., Volz, F. E., and Gainge, J. S.: 1972, 'Optical Properties of the Atmosphere', 3rd ed. AFCRL-72-0487, 113 pp.

Munro, D. S. and Davies, J. A.: 1978, 'On Fitting the Log-linear Model to Wind Speed and Temperature Profiles over a Melting Glacier', *Boundary-Layer Meteorol.* **15**, 423–437.

Oerlemans, J. and van der Veen, C. J.: 1984, *Ice Sheets and Climate*, D. Reidel Publishing Company, Dordrecht, 217 pp.

Oerlemans, J. and Fortuin, J. P. F.: 1992, 'Sensitivity of Glaciers and Small Ice Caps to Greenhouse Warming', *Science* **258**, 115–117.

Oerlemans, J. and Vugts, H. F.: 1993, 'A Meteorological Experiment in the Melting Zone of the Greenland Ice Sheet', *Bull. Am. Meteorol. Soc.* **74**(3), 355–365.

Oerlemans, J.: 1993, 'Possible Changes in the Mass Balance of the Greenland and Antarctic Ice Sheets and Their Effects on Sea Level', in Warrick, Barrow and Wigley (eds.), *Climate and Sea Level Change*, Cambridge, U.K.

Ohata, T., Kobayashi, S., Ishikawa, N., and Kawaguchi, S.: 1985, 'Structure of the Katabatic Winds at Mizuho Station, East Antarctica', *J. Geophys. Res.* **90**, 10651–10658.

Ohata, T.: 1989a, 'Katabatic Wind on Melting Snow and Ice Surfaces – I: Stationary Glacier Wind on a Large Maritime Glacier', *J. Met. Soc.Japan* **67**(1), 99–112.

Ohata, T.: 1989b, 'The Effect of Glacier Wind on Local Climate, Turbulent Heat Fluxes and Ablation', *Zeitschrift für Gletscherkunde und Glazialgeologie* **25**, 49–68.

Ohmura, A.: 1987, 'New Temperature Distribution Maps for Greenland', *Zeitschrift für Gletscherkunde und Glazialgeologie* **23**, 1–45.

Parish, T. R. and Waight, K. T.: 1987, 'The Forcing of Antarctic Katabatic Winds', *Mon. Wea. Rev.* **115**, 2214–2226.

Parish, T. R. and Bromwich, D. H.: 1991, 'Continental-scale Simulation of the Antarctic Katabatic Wind Regime', *J. Climate* **4**, 135–146.

Pettré, P. and André, J. C.: 1991, 'Surface Pressure Change Through Loewe's Phenomena and Katabatic Flow Jumps: Study of Two Cases in Adélie Land, Antarctica', *J. Atmos. Sci.* **48**(4), 557–571.

Putnins, P.: 1970, 'The Climate of Greenland', in S. Orvig (ed.), *World Survey of Climatology, the Climate of the Polar Regions*, Vol. 17. Elsevier, Amsterdam.

Schwerdtfeger, W.: 1972, 'The Vertical Variation of the Wind Through the Friction-Layer over the Greenland Ice Cap', *Tellus* **XXIV**(1), 13–16.

Sorbjan, Z., Kodama, Y., and Wendler, G.: 1986, 'Observational Study of the Atmospheric Boundary Layer over Antarctica', *J. Climate Appl. Meteorol.* **25**, 641–651.

Stenning, A. J., Banfield, C. E., and Young, G. J.: 1981, 'Synoptic Controls over Katabatic Layer Characteristics above a Melting Glacier', *J. Climatol.* **1**, 309–324.

Streten, N. A., Ishikawa, N., and Wendler, G.: 1974, 'Some Observations of the Local Wind Regime on an Alaskan Artic Glacier', *Arch. Met. Geoph. Biokl.* **B22**, 337–350.

Tjemkes, S. A. and Duynkerke, P. G.: 1989, 'The Nocturnal Boundary Layer: Model Calculations Compared to Observations', *J. Appl. Meteorol.* **28**, 161–175.

Van de Wal, R. S. W. and Oerlemans, J.: 1994, 'An Energy Balance Model for the Greenland Ice Sheet', *Global and Planetary Change* **9**, 115–132.

Van de Wal, R. S. W. and Russell, A. J.: 1994, 'A Comparison of Energy Balance Calculations, Measured Ablation and Meltwater Runoff near Søndre Strømfjord, West Greenland', *Global and Planetary Change* **9**, 29–38.

Van den Broeke, M. R., Duynkerke, P. G., and Oerlemans, J.: 1994, 'The Observed Katabatic Flow at the Edge of the Greenland Ice Sheet during GIMEX-91', *Global and Planetary Change*, **9**, 3–16.

Wendler, G. N. and Kodama, Y.: 1985, 'Some Results of Climatic Investigations of Adelie Land, Eastern Antarctica', *Zeitschrift für Gletscherkunde und Glazialgeologie* **21**, 319–3217.

Wendler, G., Ishikawa, N., and Kodama, Y.: 1988, 'The Heat Balance of the Icy Slope of Adélie Land, Eastern Antarctica', *J. Appl. Meteorol.* **27**, 52–65.